

# Low-power electrical impedance tomography spectroscopy

Juliana Padilha Leitzke and Hubert Zangl  
*Alpen-Adria University Klagenfurt, Klagenfurt, Austria*

Received 14 December 2018  
Revised 3 June 2019  
Accepted 4 June 2019

## Abstract

**Purpose** – This paper aims to present an approach based on electrical impedance tomography spectroscopy (EITS) for the determination of water and ice fraction in low-power applications such as autarkic wireless sensors, which require a low computational complexity reconstruction approach and a low number of electrodes. This paper also investigates how the electrode design can affect the reconstruction results in tomography.

**Design/methodology/approach** – EITS is performed by using a non-iterative method called optimal first order approximation. In addition to that, a planar electrode geometry is used instead of the traditional circular electrode geometry. Such a structure allows the system to identify materials placed on the region above the sensor, which do not need to be confined in a pipe. For the optimization, the mean squared error (MSE) between the reference images and the obtained reconstructed images was calculated.

**Findings** – The authors demonstrate that even with a low number of four electrodes and a low complexity reconstruction algorithm, a reasonable reconstruction of water and ice fractions is possible. Furthermore, it is shown that an optimal distribution of the sensor electrodes can help to reduce the MSE without any costs in terms of computational complexity or power consumption.

**Originality/value** – This paper shows through simulations that the reconstruction of ice and water mixtures is possible and that the electrode design is a topic of great importance, as they can significantly affect the reconstruction results.

**Keywords** EITS, Multi-frequency EIT

**Paper type** Research paper

## 1. Introduction

Icing can significantly affect aircraft performance, and it continues to be a safety concern in aviation. Many systems exist to avoid ice formation on the surface of aircraft or on instruments. Most systems rely only on verifying atmospheric icing conditions and flight-state parameters to see if the flight conditions are safe. This information is needed, as it can help pilots in decision-making or on a path and manner suggestion for flying based on such conditions (Pei *et al.*, 2017). Furthermore, heating systems used for anti-icing and deicing can have a very high power consumption (Meier and Scholz, 2010). The correct determination of ice formation on aircraft surfaces could lead to a more intelligent system, which would increase efficiency and safety during flight.

---

© Juliana Padilha Leitzke and Hubert Zangl. Published by Emerald Publishing Limited. This article is published under the Creative Commons Attribution (CC BY 4.0) licence. Anyone may reproduce, distribute, translate and create derivative works of this article (for both commercial and non-commercial purposes), subject to full attribution to the original publication and authors. The full terms of this licence may be seen at <http://creativecommons.org/licences/by/4.0/legalcode>

This study has received funding from the Icelift project as part of the Take Off initiative by Österreichische Forschungsförderungsgesellschaft (FFG), which is the national funding agency for industrial research and development in Austria.



Wireless sensor networks could be used to monitor ice formation, as they can have many advantages which include weight reduction, simple maintenance and great monitoring capability (Yedavalli and Belapurkar, 2011; Schlegl *et al.*, 2015). In Leitzke *et al.* (2017), initial studies of such a system were made for a low-power pressure distribution measurement system and a similar setup could also be used for ice detection.

Ice can be formed in different ways in nature, and it can also comprise a mixture of water molecules in liquid and solid states. In this paper, we use the difference between the complex permittivity of ice and water to perform electrical impedance tomography spectroscopy (EITS), which takes the frequency dependence of these electrical properties into consideration for the reconstruction. This system could have a small size because of our proposed planar electrode geometry and be easily placed on a surface for ice detection. Figure 1 illustrates the more common circular electrode geometry with the electrodes in black placed around a pipe, and Figure 2 illustrates a less common planar electrode geometry. For aircraft icing, planar topologies are mandatory, as the system needs to be installed on the surface of the aircraft, e.g. the aircraft wings.

The electrode design can significantly affect the reconstruction results in any tomography application. Therefore, a method should be used for optimizing the electrode configuration. In this paper, we optimize the electrode design based on the minimum mean squared error (MSE) between the reconstructed images and the reference images.

## 2. Background

Many concepts are brought together in this paper and some background on these topics is presented below. First, the issue of icing in aviation is briefly explained, such as currently used and developed systems. The definition of complex permittivity of ice and water, such as the model used for ice and water mixtures is also explained, followed by a literature review on EITS and electrode optimization.

### 2.1 Icing in aviation

Three of the most common causes of icing during flight are contamination of the aircraft's surface before taking off and encountering supercooled water droplets and ice crystals.

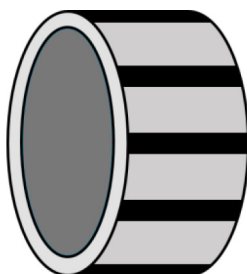


**Figure 1.**  
Common circular  
electrode geometry  
for eight electrodes



**Figure 2.**  
Symmetrical planar  
electrode geometry  
for four electrodes

According to the environmental conditions encountered during flight, different types of ice can be formed, such as rime ice, glaze ice or mixed ice (Cao *et al.*, 2018).

Ice formation on an aircraft surface can be dangerous, as it can significantly affect performance by, for example, increasing drag, decreasing lift, affecting stability or blocking vital instruments. Icing remains one of the major external causes of accidents, recently (Cao *et al.*, 2018), and many systems have been developed to avoid it.

Icing conditions should be avoided, as they can be dangerous during flight. However, because of the increasing air traffic, it is possible that aircraft cannot easily avoid such conditions, as path deviation during flight might become harder to be authorized by air traffic control due to constraints imposed by the required safety distance with respect to other aircraft.

In Caliskan *et al.* (2008), a control system based on Kalman filtering and neural networks is developed to evaluate icing according to sensor data and flight dynamics, and the system was verified in two different aircraft models in which it was demonstrated that fuel could be saved because of the automatic control of existing anti-ice systems.

Incorrect pilot manipulation is one of the factors that contributes the most to fatal icing accidents, including not paying enough attention to performance changes, using auto-pilot in icing areas, no timely opening deicing equipment or opening flaps with ice accretions for approaching (Cao *et al.*, 2018).

We propose a concept to improve the results obtained in Schlegl *et al.*'s. (2015) study of a low-cost sensor that could identify a layer of ice formed on the aircraft surface by using impedance spectroscopy. The proposed sensor could help existing systems to act and raise pilot awareness.

### 2.2 Complex permittivity of ice and water

The electrical characteristics of materials change over frequency and can be used to identify different substances which behave in a different way. Water changes its characteristics as it turns into ice, and that can be used to identify the presence of one or the other.

In Figures 3 and 4, the permittivity of ice and water is shown for different frequencies ranging from 1 Hz to 1 PHz, according to a model presented in Petrenko and Whitworth (1999). The different relaxation times between water and ice can be clearly seen on the frequency spectrum.

The complex permittivity is defined by:

$$\varepsilon = \varepsilon' + i\varepsilon'' \tag{1}$$

where the real permittivity  $\varepsilon'$  is:

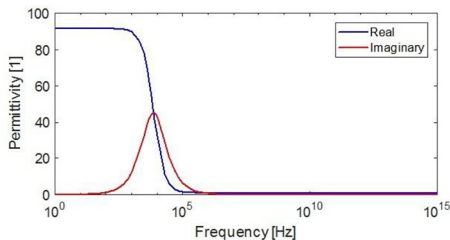


**Figure 3.**  
Real and imaginary  
permittivity of ice

$$\epsilon' = \epsilon_\infty + \frac{\epsilon_s - \epsilon_\infty}{1 + \omega^2 \tau_D^2} \quad (2)$$

The imaginary permittivity  $\epsilon''$  is:

$$\epsilon'' = \frac{\omega \tau_D (\epsilon_s - \epsilon_\infty)}{1 + \omega^2 \tau_D^2} \quad (3)$$

where  $\epsilon_s$  is the static permittivity,  $\epsilon_\infty$  is the high frequency permittivity,  $\omega$  is the angular frequency and  $\tau_D$  is the relaxation time.

### 2.3 Ice and water mixtures

Many theories have been developed to determine the permittivity of a complex electromagnetic medium as a homogeneous effective medium.

According to the Maxwell-Garnett mixing formula, in a mixture where ice is the host medium and has water inclusions of volume fraction  $f$ , the resultant permittivity is given by equation (4), where  $\epsilon_w$  is the permittivity of water and  $\epsilon_i$  is the permittivity of ice.

$$\epsilon = \epsilon_i \frac{\epsilon_i + \frac{1+2f}{3} (\epsilon_w - \epsilon_i)}{\epsilon_i + \frac{1-f}{3} (\epsilon_w - \epsilon_i)} \quad (4)$$

This theory is explained in detail in Markel (2016), as well as other different approaches.

### 2.4 Electrical impedance tomography spectroscopy

Electrical impedance tomography (EIT) is the inverse problem where the impedance in a region of interest (ROI) is determined by measuring currents and voltages at the electrodes located at the boundaries (Borcea, 2002). The impedance value varies according to the material distribution in the ROI, as different materials will present different electrical properties. The inverse problem of determining the material distribution given certain boundary measurements is ill-posed as the requirements for well-posed problems, for which a unique solution that is continuously dependent on the data must exist, are not fulfilled for EIT (Holder, 2005). In particular, the low number of electrodes, the noise and the stability of the inversion are relevant in the present application. Many image reconstruction algorithms were developed to numerically reconstruct material distribution in ill-posed situations and a review can be found in Yang and Peng (2003).

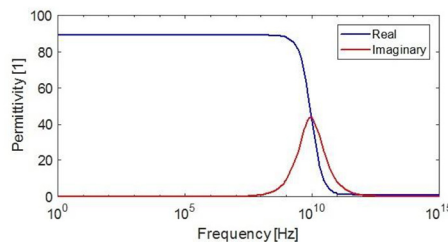


Figure 4. Real and imaginary permittivity of water

EIT might not present the best resolution, but for many applications this drawback is compensated by the possibility of being used as a small, self-powered portable system because of its comparatively low complexity design, low cost and safety of such system.

In electrical impedance spectroscopy, the frequency-dependent behavior of materials is analyzed in the frequency domain (Macdonald and Barsoukov, 2005). Some studies compare the electrical characteristics of water and ice, such as in Artemov and Volkov (2014), Longo *et al.* (2016); and Flatscher *et al.* (2017).

EITS is created by combining both approaches into one system, which is capable of reconstructing material distributions based on the frequency-dependent characteristics of different substances.

This topic was initially developed for medical applications (Griffiths and Zhang, 1989; Brown *et al.*, 1994; Griffiths and Jossinet, 1994) and it continues to be improved recently as in (Yerworth *et al.*, 2003), where measurements are made to perform EITS using frequency difference and time difference imaging methods for the reconstruction of the impedance. In Nahvi and Hoyle (2008), an EITS system is developed using a linear chirp as excitation frequency, and the image can be then obtained for each frequency of interest. An EITS method called code-division multiplexing is suggested in McEwan *et al.* (2009), and in Baidillah *et al.* (2017), a frequency-time imaging method is used together with adjacent and quasi-adjacent sensing methods.

### 2.5 Electrode optimization

Sensor design is crucial in EIT. (Yang, 2010) provides a review on the topic mainly for common circular geometries and single frequency measurement.

Electrode optimization has also been relevant in recent years, in Li and Holland (2015), the effects of different electrode aspect ratios (length divided by the diameter of the pipe) for 3D ECT reconstruction are studied for a system with 24 electrodes in a circular setup.

Considered one of the most important parts of a tomography system, the electrode optimization for ECT is also addressed in Li *et al.* (2017) for a classical circular electrode configuration, where the varied parameters were the length, width and number of electrodes. According to their results, the primary parameter is the electrode number, followed by the electrode length and then the width.

In Tholin-Chittenden and Soleimani (2017), a planar sensor topology is optimized by choosing the best design among five candidate design options proposed by the authors, where the performance of each setup was judged based on the reconstruction of a water bottle buried in sand.

## 3. Methodology

In this paper, we perform EITS by using a non-iterative method described in Zangi and Mühlbacher-Karrer (2015), called optimal first order approximation (OFOA), which is essentially an implementation of a Bayesian linear minimum mean square estimation approach. In addition to that, a planar electrode geometry is used instead of the traditional circular electrode geometry. Such a structure allows the system to identify the materials placed on the region above the sensor, which do not need to be confined in a pipe as in a common geometry where the electrodes are located around the material. To also minimize the complexity of the hardware, the number of electrodes is kept low.

### 3.1 Low power consumption

Our simulations aim at improving the ice detection results from a system initially proposed in [Schlegl et al. \(2015\)](#). Low-power consumption for our application means that the system needs to harvest energy from a very small solar cell of  $10 \text{ cm}^2$ . Considering an efficiency of 10 per cent and an average irradiance of  $20 \text{ W/m}^2$  (which is a conservative assumption for outdoor applications considering the value of about  $1,000 \text{ W/m}^2$  provided by direct sunlight), 2 mW power would be supplied to the system and should be enough for its operation.

### 3.2 Simulation

A self-written finite element method (FEM) software based on the partial differential equation toolbox on MATLAB 2017 and an open-source tool for image generation were used for the simulations, and to get a better efficiency according to simulation time, the mesh was adjusted to have a structured shape which decreases its element sizes as they get closer to the electrodes. In addition to that, the mesh was altered to have more nodes of the FEM discretization closer to the electrodes, allowing a better resolution for the sensor optimization. Even though this may not be the optimal mesh geometry, it is simple and it keeps the simulation time low for obtaining the large number of measurement samples for all frequencies.

For the generation of the prior distribution, two circular objects of random size, random center position, random ice fraction and random water fraction were created for each image. The permittivity of these objects was defined as in [equation \(4\)](#), and the fraction value could vary from pure ice to pure water. The ROI is defined as the region above the electrodes and it has a total of 5 cm in the  $x$ -axis and 3.5 cm in the  $y$ -axis, which is a suitable size with respect to the interesting layers for aircraft icing.

Measurements were made for discrete frequencies varying between 100 Hz and 1 MHz, with one measurement per decade. The measurement matrices were formed considering the measurements between all the electrodes at all frequencies, as each one of them transmits a signal separately and the others receive this signal.

### 3.3 Reconstruction

In this paper, the OFOA method is used for the reconstruction because of its low computational complexity, which makes it in particular attractive for ultra-low-power wireless sensors. It is given by:

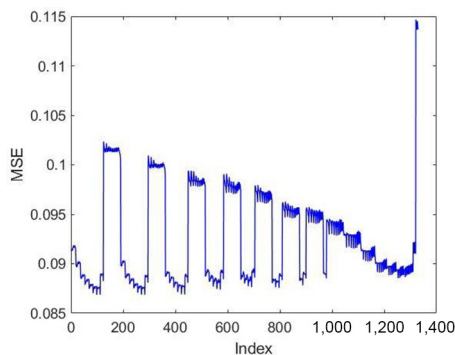


**Figure 5.**  
MSE for different  
electrode  
configurations

$$\hat{f} = Wy + B \tag{5}$$

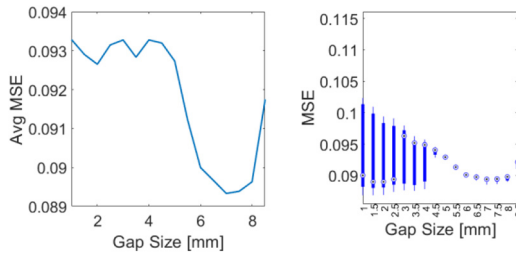
$$W = C_{fy}C_{yy}^{-1} \tag{6}$$

$$B = \bar{f} - W\bar{y} \tag{7}$$

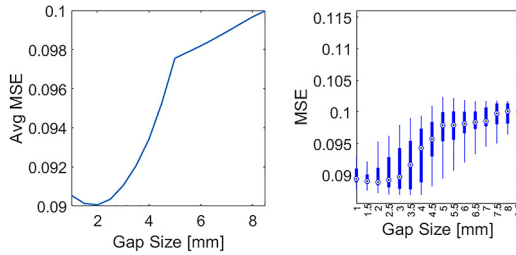
where  $C_{yy}$  is the auto-covariance matrix of the measurements,  $C_{fy}$  is the cross-covariance matrix between the measurements and the permittivities,  $\bar{f}$  is the expected value of the ice or water fraction prior to the observation,  $\hat{f}$  the estimate for the ice fraction,  $\bar{y}$  the expected value of the measurements and  $y$  the obtained measurements.

Considering a total of 25,000 FEM simulations of random samples drawn from the prior distribution, 80 per cent of these data are used for estimating the covariance matrices and consequently the OFOA reconstruction coefficients, and 20 per cent is used for testing

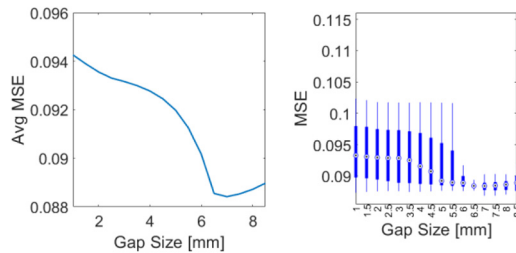
**Figure 6.**  
Average MSE and  
boxplot for different  
sizes of the first gap

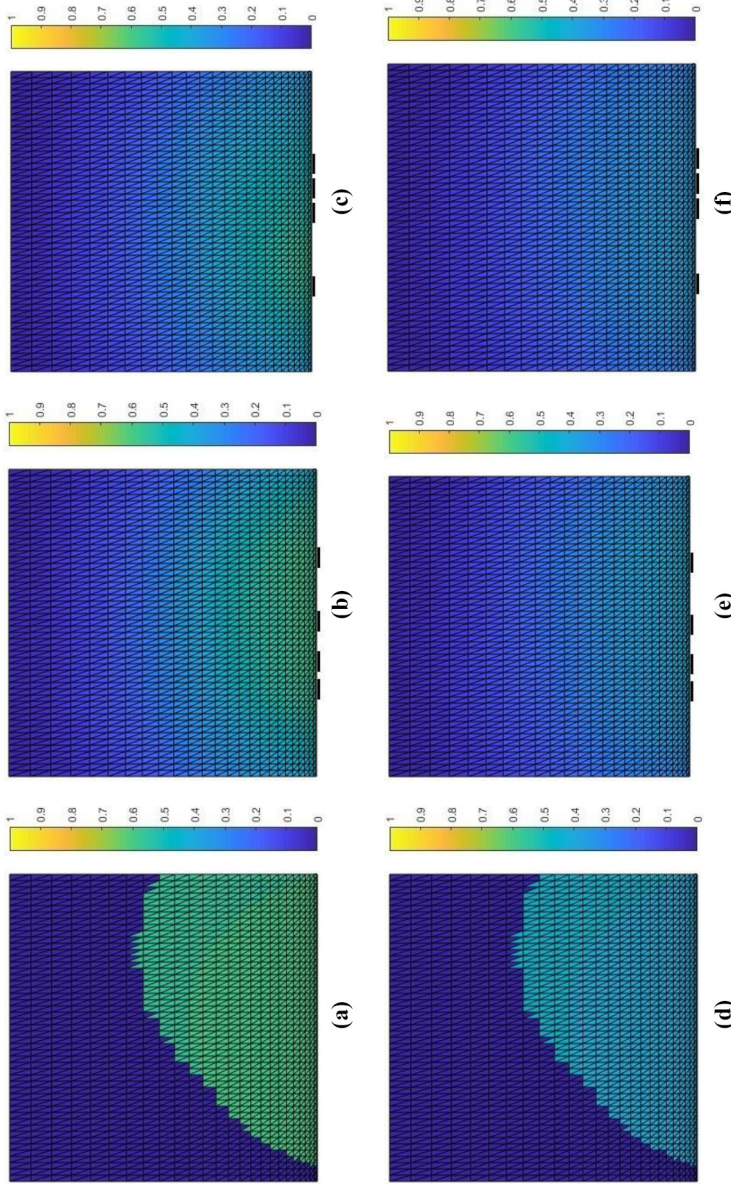


**Figure 7.**  
Average MSE and  
boxplot for different  
sizes of the second gap



**Figure 8.**  
Average MSE and  
boxplot for different  
sizes of the third gap

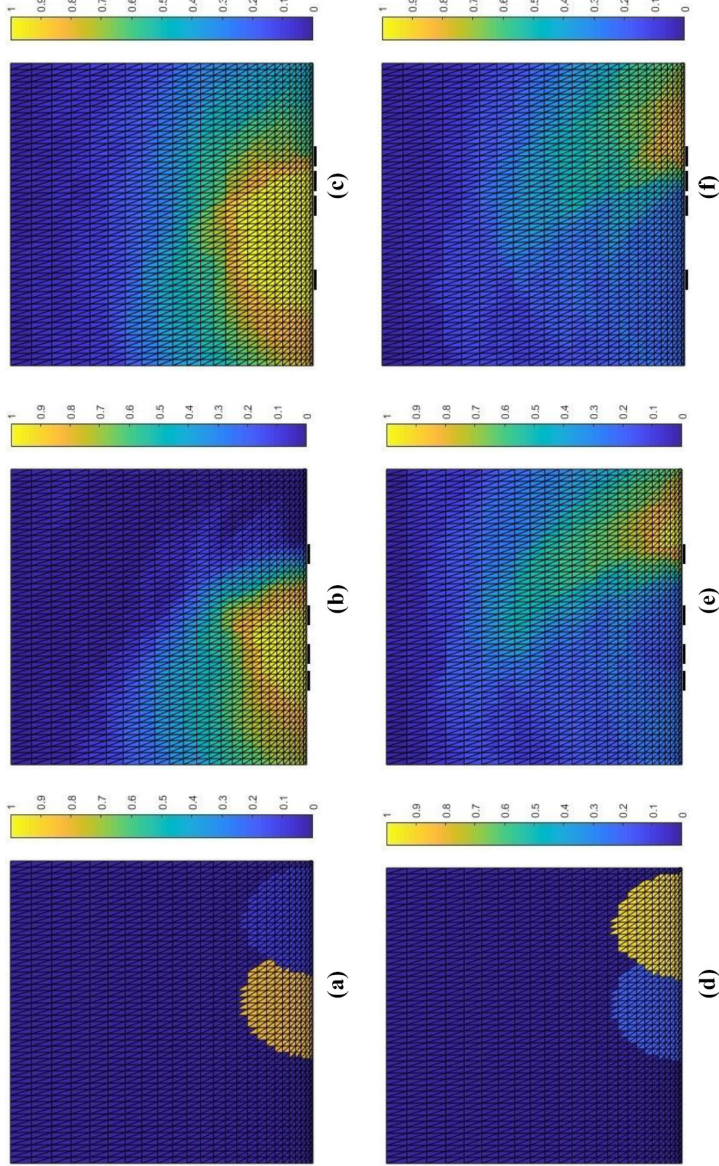




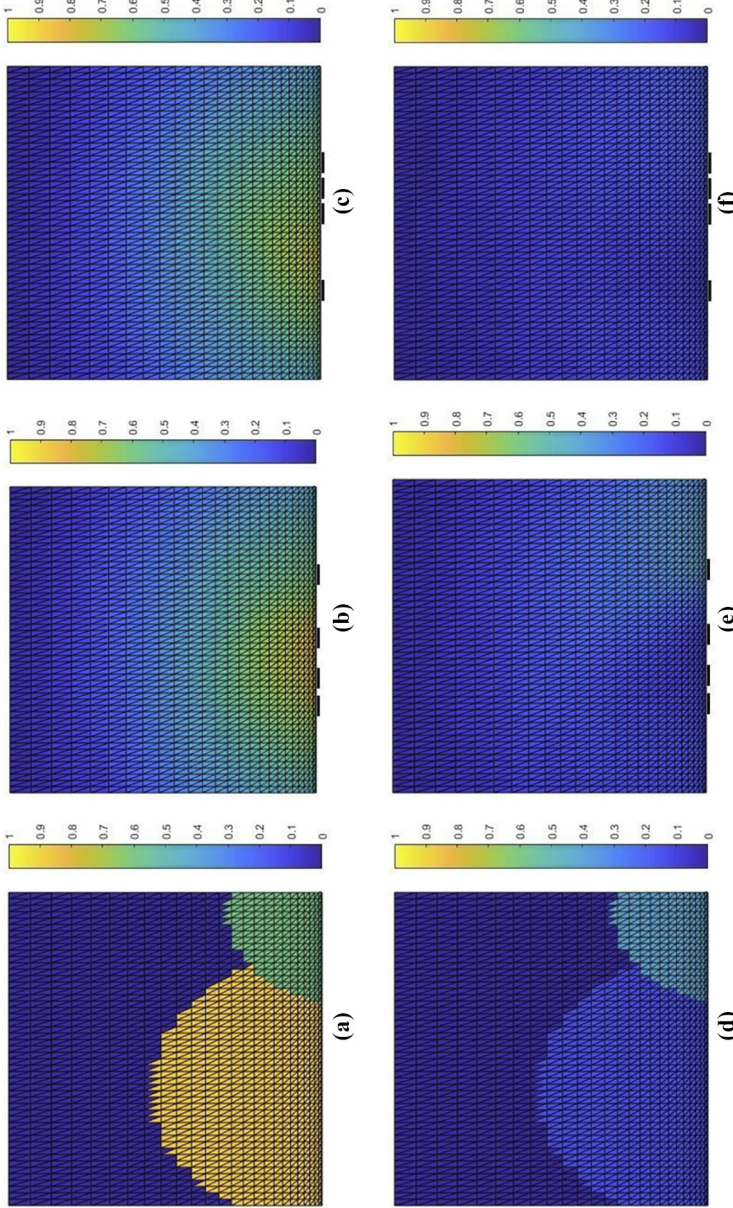
**Notes:** The position of the four planar electrodes is shown below the reconstructed images in black. The material fraction is presented as a percentage value, here varying between 0 and 1

**Figure 9.** Reference image for (a) water and (d) ice fractions, (b) water fraction reconstruction for optimal electrode configuration, (c) water fraction reconstruction for configuration with higher MSE, (e) ice fraction reconstruction for optimal electrode configuration and (f) ice fraction reconstruction for configuration with higher MSE

**Figure 10.** Reference image for (a) water and (d) ice fractions, (b) water fraction reconstruction for optimal electrode configuration, (c) water fraction reconstruction for configuration with higher MSE, (e) ice fraction reconstruction for optimal electrode configuration and (f) ice fraction reconstruction for configuration with higher MSE



**Notes:** The position of the four planar electrodes is shown below the reconstructed images in black. The material fraction is presented as a percentage value, here varying between 0 and 1



**Notes:** The position of the four planar electrodes is shown below the reconstructed images in black. The material fraction is presented as a percentage value, here varying between 0 and 1

**Figure 11.** Reference image for (a) water and (d) ice fractions, (b) water fraction reconstruction for optimal electrode configuration, (c) water fraction reconstruction for configuration with higher MSE, (e) ice fraction reconstruction for optimal electrode configuration and (f) ice fraction reconstruction for configuration with higher MSE

purposes, optimization and error calculation. Gaussian noise in the order of fF was added to all measurement data obtained from the simulations.

3.4 Optimization

For the optimization, the MSE between the  $N$  reference images and the obtained reconstructed images was calculated using equation (8), where  $X_W$  is the matrix containing the pixel values in the reference images for the water fraction,  $X_I$  is the matrix containing the pixel values in the reference images for the ice fraction,  $Y_W$  the matrix which contains the pixel values obtained with the reconstructions for the water fraction and  $Y_I$  the matrix obtained with the reconstructions for the ice fraction.

$$MSE = \frac{1}{N} \sum_{j=1}^N \left[ (Y_{W_j} - X_{W_j})^2 + (Y_{I_j} - X_{I_j})^2 \right] \tag{8}$$

Even though the performance of the system could be increased with a larger number of electrodes (Yang, 2010), we used a configuration with only four electrodes. The reason for this is that we were aiming for wireless sensors, and we therefore wanted to minimize the complexity of the electronic circuitry and the power consumption for the measurement. The number of electrodes was selected based on a compromise between measurement time (and energy) and available data. While two electrodes would only have one independent measurement per frequency, for reconstructing the material distribution, therefore, more than three electrodes should be used. While three electrodes generate three independent measurements, four will generate six independent measurements. As with only one more electrode it is possible to double the measurement matrix, this was chosen as a compromise for the number of electrodes for this investigations.

The position of the four electrodes was varied along the center region of the ROI using the FEM simulations results. For each new sensor geometry, the MSE was calculated and the geometry which presented the minimum MSE was considered optimal.

4. Results

For all configurations, the MSE is calculated according to equation (8), and the results are shown in Figure 5. Each index represents a possible electrode setup.

It was expected that the symmetrical configuration would achieve the best MSE, as this is what is widely used in the literature. However, as seen on Table I below, such configuration presented an MSE of 0.09406 in comparison to 0.08685 obtained for the optimal geometry. When we consider the mirrored setup of the optimal geometry (the same distances but in inverted order), we also get a similar result as expected with an MSE of 0.08896. Even though the reduction of the MSE may not appear dramatic, it should be noted that it comes for free in terms of measurement complexity and computational complexity.

**Table I.**  
Electrode geometry  
and MSE

Geometry	MSE
Optimal (lowest MSE)	0.08685
Optimal mirrored	0.08896
Symmetrical	0.09406
Highest MSE	0.1147

In Figures 6, 7 and 8, the average MSE value for each of the three gaps between the four electrodes is shown with respect to that gap's size, as well as the box plot, which indicates a size for each gap that would tend to reduce the total MSE.

The reconstruction results for the optimal electrode configuration and for a configuration with higher MSE can be seen in Figure 9. Other examples are shown in Figures 10 and 11. The ice and water fractions of a specific material distribution are reconstructed resulting in two images, which are complementary and can vary between 0 and 1.

Even if the difference in MSE does not appear to be much, it is clear that this can make a difference in the reconstruction results. This can be seen, for example, in Figure 11, where the fraction of ice is not detected when the geometry with higher MSE is used and it can be detected by the geometry with low MSE.

## 5. Conclusion

In this paper, we present an approach to obtain an estimate of the spatial distribution of water and ice fraction (i.e. wet ice or snow), which is of interest in many industrial processes and also in the control of anti-icing systems on aircraft.

We demonstrate that even with a low number of four electrodes and a low complexity reconstruction algorithm, a reasonable reconstruction of water and ice fractions is possible. Furthermore, it is shown that an optimal distribution of the sensor electrodes can help to reduce the MSE without any costs in terms of computational complexity or power consumption. Such an approach has the potential to be used with autarkic (i.e. self sustained) wireless sensors, e.g. for the application on aircraft wings, turbines or sensors.

## References

- Artemov, V. and Volkov, A. (2014), "Water and ice dielectric spectra scaling at 0 C", *Ferroelectrics*, Vol. 466 No. 1, pp. 158-165.
- Baidillah, M., Iman, A-A., Sun, Y. and Takei, M. (2017), "Electrical impedance spectro-tomography based on dielectric relaxation model", *IEEE Sensors Journal*, Vol. 17 No. 24.
- Borcea, L. (2002), "Electrical impedance tomography", *Inverse Problems*, Vol. 18 No. 6, p. R99.
- Brown, B., Barber, D., Wang, W., Lu, L., Leathard, A., Smallwood, R., Hampshire, A., Mackay, R. and Hatzigalanis, K. (1994), "Multi-frequency imaging and modelling of respiratory related electrical impedance changes", *Physiological Measurement*, Vol. 15 No. 2, p. A1.
- Caliskan, F., Aykan, R. and Hajiyev, C. (2008), "Aircraft icing detection, identification, and reconfigurable control based on kalman filtering and neural networks", *Journal of Aerospace Engineering*, Vol. 21 No. 2, pp. 51-60.
- Cao, Y., Tan, W. and Wu, Z. (2018), "Aircraft icing: an ongoing threat to aviation safety", *Aerospace Science and Technology*, Vol. 75.
- Flatscher, M., Neumayer, M. and Brettertklieber, T. (2017), "Field sensor analysis for electrical impedance spectroscopy based ice detection", *In SENSORS, 2017 IEEE*.
- Griffiths, H. and Jossinet, J. (1994), "Bioelectrical spectroscopy from multi-frequency eit", *Physiological Measurement*, Vol. 15 No. 2, p. A59.
- Griffiths, H. and Zhang, Z. (1989), "A dual-frequency electrical impedance tomography system", *Physics in Medicine and Biology*, Vol. 34 No. 10, p. 1465.
- Holder, D.S. (2005), *Electrical Impedance Tomography*, 1st ed., Institute of Physics Publishing: Bristol and Philadelphia.
- Leitzke, J.P., Della Mea, A., Faller, L.-M., Mühlbacher-Karrer, S. and Zangl, H. (2017), "Wireless differential pressure measurement for aircraft", *Measurement*.

- Li, Y. and Holland, D.J. (2015), "Optimizing the geometry of three-dimensional electrical capacitance tomography sensors", *IEEE Sensors Journal*, Vol. 15 No. 3, pp. 1567-1574.
- Li, N., Cao, M., He, C., Wu, B., Jiao, J. and Yang, X. (2017), "Multi-parametric indicator design for ECT sensor optimization used in oil transmission", *IEEE Sensors Journal*, Vol. 17 No. 7, pp. 2074-2088.
- Longo, J.P.N., Leitzke, J.P., Morales, R.E. and da Silva, M.J. (2016), "Simple measuring system for impedance spectroscopy analysis of fluids", in *Instrumentation Systems, Circuits and Transducers (INSCIT), International Symposium on, IEEE*, pp. 77-80.
- McEwan, A., Tapson, J., vanSchaik, A. and Holder, D.S. (2009), "Code-division-multiplexed electrical impedance tomography spectroscopy", *IEEE Transactions on Biomedical Circuits and Systems*, Vol. 3 No. 5, pp. 332-338.
- Macdonald, J.R. and Barsoukov, E. (2005), *Impedance Spectroscopy: theory, Experiment, and Applications*, Wiley.
- Markel, V.A. (2016), "Introduction to the Maxwell Garnett approximation: tutorial", *Journal of the Optical Society of America A*, Vol. 33 No. 7, pp. 1244-1256.
- Meier, O. and Scholz, D. (2010), *A Handbook Method for the Estimation of Power Requirements for Electrical de-Icing Systems*, DLRK, Hamburg.
- Nahvi, M. and Hoyle, B. (2008), "Wideband electrical impedance tomography", *Measurement Science and Technology*, Vol. 19 No. 9, pp. 094011.
- Pei, B., Xu, H. and Xue, Y. (2017), "Flight-safety space and cause of incident under icing conditions", *Journal of Guidance, Control, and Dynamics*, pp. 1-8.
- Petrenko, V.F. and Whitworth, R.W. (1999), *Physics of Ice*, OUP, Oxford.
- Schlegl, T., Moser, M. and Zangl, H. (2015), "Wireless and flexible ice detection on aircraft", in *International Conference on Icing of Aircraft, Engines, and Structures. SAE: Prague, Czech Republic*.
- Tholin-Chittenden, C. and Soleimani, M. (2017), "Planar array capacitive imaging sensor design optimization", *IEEE Sensors Journal*, Vol. 17 No. 24, pp. 8059-8071.
- Yang, W. and Peng, L. (2003), "Image reconstruction algorithms for electrical capacitance tomography", *Measurement Science and Technology*, Vol. 14 No. 1, pp. R1-R13.
- Yang, W. (2010), "Design of electrical capacitance tomography sensors", *Measurement Science and Technology*, Vol. 21 No. 4, p. 042001.
- Yedavalli, R.K. and Belapurkar, R.K. (2011), "Application of wireless sensor networks to aircraft control and health management systems", *Journal of Control Theory and Applications*, Vol. 9 No. 1, pp. 28-33.
- Yerworth, R.J., Bayford, R., Brown, B., Milnes, P., Conway, M. and Holder, D.S. (2003), "Electrical impedance tomography spectroscopy (EITS) for human head imaging", *Physiological Measurement*, Vol. 24 No. 2, p. 477.
- Zangl, H. and Mühlbacher-Karrer, S. (2015), "Artefact reduction in fast Bayesian inversion in electrical tomography", *Compel - the International Journal for Computation and Mathematics in Electrical and Electronic Engineering*, Vol. 34 No. 5, pp. 1381-1391.

**Corresponding author**

Juliana Padilha Leitzke can be contacted at: [juliana.leitzke@aau.at](mailto:juliana.leitzke@aau.at)

For instructions on how to order reprints of this article, please visit our website:

[www.emeraldgroupublishing.com/licensing/reprints.htm](http://www.emeraldgroupublishing.com/licensing/reprints.htm)

Or contact us for further details: [permissions@emeraldinsight.com](mailto:permissions@emeraldinsight.com)